Available online at www.sciencedirect.com
SCIENCE DIRECT®
Journal of Hydrology 310 (2005) 157–180
Journal of Hydrology
www.elsevier.com/locate/jhydrol

Signatures in flowing fluid electric conductivity logs

Christine Doughty*, Chin-Fu Tsang[1]

Earth Sciences Division, E.O. Lawrence Berkeley National Laboratory, University of California, 1 Cyclotron Road, MS 90-1116 Berkeley, CA 94720, USA

Received 4 December 2003; revised 9 December 2004; accepted 14 December 2004

Abstract

Flowing fluid electric conductivity logging provides a means to determine hydrologic properties of fractures, fracture zones, or other permeable layers intersecting a borehole in saturated rock. The method involves analyzing the time-evolution of fluid electric conductivity (FEC) logs obtained while the well is being pumped and yields information on the location, hydraulic transmissivity, and salinity of permeable layers. The original analysis method was restricted to the case in which flows from the permeable layers or fractures were directed into the borehole (inflow). Recently, the method was adapted to permit treatment of both inflow and outflow, including analysis of natural regional flow in the permeable layer. A numerical model simulates flow and transport in the wellbore during flowing FEC logging, and fracture properties are determined by optimizing the match between simulation results and observed FEC logs. This can be a laborious trial-and-error procedure, especially when both inflow and outflow points are present. Improved analyses methods are needed. One possible tactic would be to develop an automated inverse method, but this paper takes a more elementary approach and focuses on identifying the signatures that various inflow and outflow features create in flowing FEC logs. The physical insight obtained provides a basis for more efficient analysis of these logs, both for the present trial and error approach and for a potential future automated inverse approach. Inflow points produce distinctive signatures in the FEC logs themselves, enabling the determination of location, inflow rate, and ion concentration. Identifying outflow locations and flow rates typically requires a more complicated integral method, which is also presented in this paper.

Keywords: Borehole logging; Fluid electric conductivity logging; Hydraulically conductive fractures; Heterogeneous aquifers; Hydrogeologic characterization; Flow and transport modeling

1. Introduction

In the study of flow and transport through fractured rocks, knowledge of the locations of fractures and their hydraulic properties is essential. Often such knowledge is obtained using deep boreholes penetrating the fractured rock. Of the various downhole methods for determining fracture flow that have been

* Corresponding author. Tel.: +1 510 486 6453; fax: +1 510 486 4159.
E-mail addresses: cadoughty@lbl.gov (C. Doughty), cftsang@lbl.gov (C.-F. Tsang).
[1] Tel.: +1 510 486 5782; fax: +1 510 486 5686.

0022-1694/$ - see front matter © 2005 Elsevier B.V. All rights reserved.
doi:10.1016/j.jhydrol.2004.12.003

developed over the past few decades (National Research Council Committee on Fracture Characterization and Fluid Flow, 1996, Chapter 4), flowing fluid electric conductivity (FEC) logging has proven to be quite successful. Since Tsang et al. (1990) introduced the method, it has been applied in deep wells to depths of 1500 m or more (Kelley et al., 1991; Guyonnet et al., 1993), in inclined boreholes drilled in the underground Grimsel Test Laboratory (Marschall and Vomvoris, 1995), and extensively in shallower wells of 100 m or less (Evans et al., 1992; Pedler et al., 1992; Bauer and LoCoco, 1996; Paillet and Pedler, 1996; Karasaki et al., 2000). In the flowing FEC logging method, wellbore water is first replaced by de-ionized water or, alternatively, water of a constant salinity distinctly different from that of the formation water. This is done by passing the de-ionized water down a tube to the bottom of the borehole at a given rate, while simultaneously pumping from the top of the well at the same rate, until the FEC of the water pumped out of the well stabilizes at a low value. Next, the well is shut in (i.e. pumping is stopped) and the tubing is removed. Then the well is pumped, usually from the top, at a constant low flow rate (e.g. tens of liters per minute), while an electric conductivity probe is lowered into the borehole to record the FEC as a function of depth. This produces what is known as a flowing FEC log. With constant pumping conditions, a series of five or six flowing FEC logs are typically obtained over a one- or two-day period, dependent on the length of well section being studied. At depth locations where water enters the borehole (the feed points), the flowing FEC logs display peaks. These peaks grow with time and are skewed in the direction of water flow. By analyzing these logs at successive times, it is possible to obtain the flow rate and salinity of groundwater inflow to the wellbore from individual hydraulically conductive fractures.

Using an electric conductivity probe to produce an FEC log is a simple technique that does not require novel equipment or procedures, and has long been used to characterize subsurface heterogeneity (e.g. Keys, 1989; Aquilina et al., 1996; Ward et al., 1998). The essential advantage of the flowing FEC logging method lies in the context in which the probe is used. By beginning with a wellbore filled with contrasting salinity water (e.g. de-ionized water) and maintaining a constant pumping rate during logging, the sequence of FEC logs monitors a dynamic flow and transport response that depends on the hydraulic properties and salinity of the formation. In contrast, standard static FEC (or resistivity) logs reflect variations in formation salinity, but provide no information on flow conditions.

Furthermore, under a wide range of conditions, the flowing FEC logging method has been found to be more accurate than spinner flow meters and much more efficient and less costly than packer tests, the two traditional means of assessing hydraulic transmissivity (Tsang et al., 1990; Paillet and Pedler, 1996; Karasaki et al., 2000). Spinner flow meters are very sensitive to variations in wellbore radius, because they measure a local fluid velocity that is inversely proportional to wellbore radius squared. In contrast, fluid FEC logging provides a more integrated measure of fluid velocity in the well, as reflected by the movement of FEC peaks, making it less sensitive to minor variations in wellbore radius. However, large washout zones may create fluid velocity changes that introduce spurious effects into the FEC logs. Engineered changes in wellbore radius (e.g. due to drilling bit size changes) also affect the fluid velocity in the wellbore, but these may be accounted for explicitly in the analysis if their depth and magnitude are known.

Packer tests are very labor- and time-intensive, because they require packers to be set above and below each depth interval in the borehole to be tested. Once the packers are set, one must wait for wellbore pressure to become steady, then the well is pumped and the pressure-transient recorded. Ideally, pumping continues until pressure becomes steady again. Then, the packers are deflated, moved to a new depth interval, and the process repeated. Choosing the depths at which to set the packers can be problematic: if depth intervals are too wide, multiple fractures may not be resolved, whereas if they are too narrow, a high proportion of depth intervals may include no fractures at all. It has been suggested (Cohen, 1995) that packer tests are not well suited for identifying fracture locations, but are good at assessing fracture transmissivities after fracture locations have been found by some other method. Under some non-ideal conditions (e.g. very low-permeability fractures, flow systems with boundaries or strongly different flow geometries within different fractures), the pressure-transient analysis done for a packer test can provide more

useful information than can flowing FEC logging. In general, the two methods may be considered to be complementary rather than alternatives.

Although feed points are presented in this paper as representing flow through hydraulically transmissive fractures, they can also represent flow through any permeable zone that intersects the wellbore section being logged. For example, in heterogeneous porous media such as alluvial systems composed of interspersed sand and clay lenses, flow can be just as localized as in fractured rock, and the need for identifying permeable strata just as great. The method developed in this paper is equally applicable to such media.

Fig. 1 shows a typical example of a series of flowing FEC logs obtained from a 230 m deep well that is being pumped from the bottom, collected over a period of about four hours (Colog, Inc., personal communication, 1999). Although it is usually simplest to pump from the top of the well, the pump can be located either at the top or the bottom of the wellbore interval being studied. For situations in which one feed point is much stronger than all the others, alternative pump locations may facilitate identifying the smaller feed points, by drawing flow from the large feed point away from them. Logging data are obtained while the tool moves both up and down the wellbore, but due to the design of the measurement point within the probe, FEC profiles obtained during upward logging correspond to water flow in a less optimal pattern around the measurement point, and are generally not used. Key features apparent in the logs include (a) an isolated peak at a depth of 164 m with a sharp upper limb; (b) several interfering peaks in the depth range of 174–187 m; and (c) an overall downward propagation of peaks. The goal of the present study is to investigate the typical signatures exhibited in flowing FEC logs that are produced by different combinations of feed points and flow conditions. Further, integral measures will be derived from the FEC logs, to facilitate analysis of flow conditions that do not produce a strong signature in the FEC logs themselves.

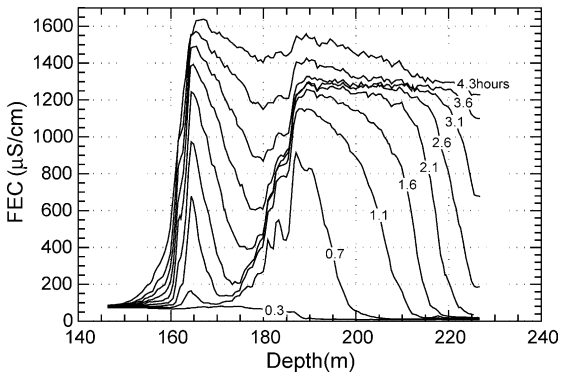

Fig. 1. Example of flowing FEC logs (Colog, Inc., personal communication, 1999).

Existing tools for analyzing flowing FEC logs include analytical solutions, numerical modeling, and integral approaches. Simple analytical solutions based on mass balances can be used to infer feed-point properties at early times before peaks interfere with each other (Tsang et al., 1990); under steady-state conditions when peaks fully interfere (Tsang et al., 1990); and for the special case of horizontal flow (Drost et al., 1968). These solutions provide useful information when used as part of a more sophisticated analysis (as described in Section 2), but by themselves are too simplistic for most real-world problems.

The numerical model BORE (Hale and Tsang, 1988; Tsang et al., 1990) and the recently enhanced version BORE II (Doughty and Tsang, 2000) calculate the time evolution of ion concentration (salinity) through the wellbore, given a set of feed-point locations, strengths, and concentrations (i.e. the forward problem). BORE II broadens the range of applicability of the analytical solutions described above by considering multiple inflow and outflow feed points, isolated and overlapping FEC peaks, early-time and late-time behavior, time-varying feed-point strengths and concentrations, and the interplay of advection and dispersion in the wellbore. The Appendix A presents the governing equations used by BORE II. Using BORE II to match observed FEC profiles (the inverse problem) requires the trial-and-error adjustment of feed-point parameters (i.e. the location, strength, and concentration of each feed point). The inverse problem for individual inflow feed points is formally well posed, with location, strength, and concentration all producing distinct effects on the FEC logs. In contrast, outflow feed points produce no effect of their own, but greatly alter the FEC peaks created by adjacent inflow points. Consequently, parameter adjustment can be a difficult and time-consuming process, especially for noisy data.

Several integral approaches have been developed (Tsang and Hale, 1989; Löw et al., 1990; 1994) that can provide good initial guesses to BORE, greatly enhancing its ease of use. Additionally, Evans (1995) has formalized the inversion process with an automated search for the feed-point parameters that minimize the misfit between modeled and observed FEC profiles. However, these methods are limited to wellbore sections containing only inflow points. Thus, they are not applicable to cases of horizontal flow across the wellbore diameter or internal wellbore flow, two manifestations of the co-existence of inflow and outflow feed points. Simply extending Evans' (1995) automated search method to systems including both inflow and outflow feed points could prove problematic because the outflow feed points do not produce a direct effect on the FEC logs.

This paper focuses on identifying and understanding the various features created by inflow and outflow points that may appear in the FEC logs, which are denoted as feed-point signatures. Developing an understanding of feed-point signatures is a necessary step for efficient analysis of flowing FEC logs, whether done by trial and error or within an automated inverse method. The present paper is based upon theoretical developments described in three previous papers by the authors. First, Tsang et al. (1990) introduced the concept of flowing FEC logging, but limited the application to inflow points. Second, Doughty and Tsang (2000) generalized the analysis method to include inflow and outflow points. Third, Tsang and Doughty (2003) introduced the concept of multi-rate flowing FEC logging, wherein logging is repeated using different well pumping rates, as a means to learn more about the hydrologic character of inflow and outflow points. Each of these three papers took a forward approach, in which a combination of physical processes produced flowing FEC logs. In contrast, the present paper takes more of an inverse approach; that is, beginning with the FEC logs themselves, physical insight into how particular features or signatures in flowing FEC logs arise from various types of feed points is discussed. Consequently, the present paper is intended to be a practical tool for those analyzing flowing FEC logs, by developing procedures for making feed-point parameter estimates when both inflow and outflow points exist and when multiple pumping rates are used.

In Section 2, the typical signatures observed in flowing FEC logs are examined, to investigate what they reveal about the feed-point parameters. The FEC profile itself is used to study inflow points, whereas for outflow points an integral analysis is developed. Section 3 explores the effect of pumping rate on these signatures. Section 4 illustrates the application of these techniques by analyzing flowing FEC logs obtained from two field sites. Section 5 summarizes the material and presents some concluding remarks.

2. Signatures of inflow and outflow points

The signatures of individual inflow feed points and various combinations of inflow and outflow feed points in flowing FEC logs contain both qualitative and quantitative information about the feed-point parameters. As described in the previous section, inferring feed-point parameters from logs is an inverse problem. In these discussions, the concentration profile $C(z)$ is the ion concentration of borehole fluid as a function of depth z. The conversion of an FEC log to a concentration profile is described in the Appendix A.

2.1. Concentration profiles

Concentration profiles depend on four feed-point parameters: location z_i, inflow or outflow rate q_i (positive for inflow and negative for outflow), and, for inflow points, concentration C_i and the time t_{0i} at which feed-point concentration first differs from the initial wellbore concentration C_0. Often $t_{0i}=0$, but a non-zero value can occur if de-ionized water migrates into the fracture during the initialization phase of replacing borehole water prior to wellbore logging, or if wellbore logging is conducted as part of the monitoring effort during a tracer test in which a saline tracer arrives from a nearby well or source.

2.1.1. Inflow points

Fig. 2 shows a series of idealized concentration profiles simulated with the numerical model BORE II for a well pumped from the top, containing feed points with constant $q_i>0$, constant C_i, $C_0=0$, and $t_{0i}=0$.

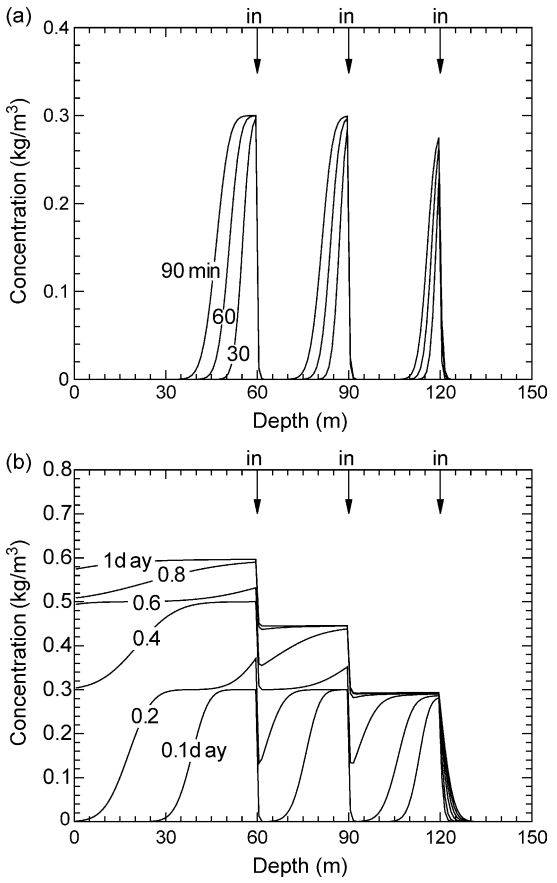

Fig. 2. Simulated concentration profiles for three inflow feed points: (a) at early times before peaks interfere; and (b) at later times, including near steady-state conditions.

Feed-point properties z_i, q_i, and C_i values are given in Table 1. Factors such as time-dependent feed points, inflow points with $C_i = C_0$, and outflow points are discussed separately in later subsections.

The first step in the feed-point characterization is to identify feed-point locations. Inflow points can usually be located fairly accurately from early-time concentration profiles, when each inflow point produces a small, isolated concentration peak. In the example shown in Fig. 2, inflow points are apparent at depths of 60, 90, and 120 m (see also Figs. 13 and 17 for field examples).

For inflow points, the estimation of q_i and C_i is best done concurrently, because these quantities have a coupled effect on $C(z)$. For early-time data, before inflow peaks begin to interfere with each other, mass conservation requires that at time t, the ion mass represented by the ith concentration peak, $M_i(t)$, be given by

$$M_i(t) = q_i(C_i - C_0)t. \tag{1}$$

Therefore, the area under the ith $C(z)$ peak can be expressed as

$$A_i = \int [C(z) - C_0]\, \mathrm{d}z = \frac{M_i(t)}{\pi r^2} = \frac{q_i(C_i - C_0)t}{\pi r^2}, \tag{2}$$

where r is the wellbore radius. Löw et al. (1990) show that Eq. (2) holds whether or not there is flow entering the peak from below, as long as that flow has concentration C_0. Calculating A_i by numerically integrating the $C(z)$ profile in the vicinity of the ith feed point can be done at a series of times to estimate the product $q_i(C_i - C_0)$ and to verify that it is constant with time. Very early profiles, which show small peaks, generally provide less accurate integrals than do larger peaks. As a rule, the largest noninterfering peaks should be used to estimate the $q_i(C_i - C_0)$

Table 1
Feed-point parameters inferred from concentration profiles shown in Fig. 2

Parameter	How Determined	Feed Point		
		1	2	3
z (m)	Observed from early-time $C(z)$ profiles	120	90	60
qC (g/min)	Calculated from area under early-time $C(z)$ peak	0.227 (0.225)	0.462 (0.450)	0.696 (0.675)
C_{max} (g/L)	Observed from late-time $C(z)$ profiles	0.30	0.45	0.60
q (L/min)	Calculated from current C_{max} and current and deeper qC values (Eq. (5))	0.76 (0.75)	0.77 (0.75)	0.77 (0.75)
C (g/L)	Calculated from current qC and q values (Eq. (6))	0.30	0.60	0.89 (0.90)

The actual feed-point parameters used to generate the concentration profiles are shown in parentheses if they differ from the inferred values. The differences reflect numerical inaccuracies in integration and estimation procedures. For this example, $C_0 = 0$ and $Q = 2.25$ L/min.

product. Table 1 summarizes the $q_i(C_i - C_0)$ products obtained for the peaks shown in Fig. 2.

At intermediate times, flow within the wellbore causes peaks to become skewed in the direction of local in-well flow, usually toward the location of the pump (throughout this paper assumed to be at the top of the well unless otherwise specified). Such skewness can be used to separately identify q_i and C_i. This can be done by fitting FEC profiles to numerical results from BORE II in which q_i and C_i are varied, while keeping the $q_i(C_i - C_0)$ product constant.

At late times, the concentration profile reaches a steady-state condition consisting of a series of steps with concentration $C_{\max i}$, each associated with an inflow point. For the lowest inflow point (z_1, q_1, C_1) in a wellbore section closed at the bottom, the steady-state concentration $C_{\max 1}$ is equal to C_1. Mixing rules introduced by Tsang et al. (1990) dictate that the second-lowest inflow point (z_2, q_2, C_2, with $z_2 < z_1$) has $C_{\max 2}$ given by

$$C_{\max 2} = \frac{q_1(C_1 - C_0) + q_2(C_2 - C_0)}{q_1 + q_2} + C_0 = \frac{q_1 C_1 + q_2 C_2}{q_1 + q_2}. \quad (3)$$

Generally, for the ith inflow point,

$$C_{\max i} = \frac{\sum q_j(C_j - C_0)}{\sum q_j} + C_0 = \frac{\sum q_j C_j}{\sum q_j}, \quad (4)$$

where the sums are taken over all feed points with $z_j \geqq z_i$. This expression can be solved for q_i,

$$q_i = \frac{\sum q_j(C_j - C_0)}{C_{\max i} - C_0} - \sum q_k, \quad (5)$$

where the j sum is taken over all feed points with $z_j \geqq z_i$ and the k sum is taken over all feed points with $z_k > z_i$. Finally, C_i is determined from the $q_i(C_i - C_0)$ product and q_i:

$$C_i = \frac{q_i(C_i - C_0)}{q_i} + C_0. \quad (6)$$

Hence, observing $C_{\max 1}$ gives C_1, and using the value of the $q_1(C_1 - C_0)$ product from the early-time data determines q_1. Then, knowing $q_1(C_1 - C_0)$, $q_2(C_2 - C_0)$, q_1, and $C_{\max 2}$ determines q_2 and C_2. Continuing this way up the wellbore section determines all feed-point properties. Table 1 summarizes the $C_{\max i}$, q_i, and C_i values for the feed points shown in Fig. 2. Note that any errors introduced at lower feed points influence the results for shallower feed points, so the accuracy of the feed-point property estimates may decrease as one moves up the wellbore.

A consistency check is provided by comparing the sum of all the feed-point inflow rates Σq_i to the pumping rate from the top of the wellbore section Q, which is a known quantity prescribed as part of the logging procedure. Assuming quasi steady-state flow conditions apply within the wellbore, then $\Sigma q_i = Q$. If this equality does not hold, there are two possible remedies. If all the feed points show equally good plateaus, then all the inflow rates can be scaled by the ratio $Q/\Sigma q_i$. However, a common situation is for logging to end before the uppermost (Nth) peak reaches steady state, in which case Q can simply be used in place of Σq_i in Eq. (4) to determine $C_{\max N}$. Note particularly that to use Q as a constraint, care must be taken that it does not include unknown contributions from inflow into the wellbore above the logged section being analyzed. This often happens in actual field conditions.

Careful examination of Fig. 2b shows that steady state (step changes in the concentration profile) is reached progressively later as one moves up the wellbore, because of the finite time it takes for the impact of the deepest peak to propagate upward. The achievement of steady-state conditions is denoted the concentration front, and it propagates wave-like up the wellbore. In Fig. 2b, the concentration front is at a depth of 90 m at 0.6 days, 60 m at 0.8 days, and about 20 m at 1 day.

If there is reason to believe that the C_i for all inflow points are the same ($C_i = C$), then Eq. (4) gives $C_{\max i} = C$, implying that steady-state concentration profiles do not provide any new information. For this special case, it is possible to determine all the q_i values and C from early-time profiles only. First, the early-time profiles are used to determine the $q_i(C - C_0)$ product for each feed point as usual. Then, the equation $Q = \Sigma q_i$ is multiplied by $(C - C_0)$ on both sides,

$$(C - C_0)Q = (C - C_0)\sum q_i = \sum q_i(C - C_0) \quad (7)$$

and solved for C

$$C = \frac{\sum q_i(C - C_0)}{Q} + C_0. \tag{8}$$

Finally, knowing $(C-C_0)$ allows q_i to be determined from the $q_i(C-C_0)$ product.

Another simplification can be realized if the feed points are far enough apart for $C(z)$ plateaus to develop before the peaks begin to interfere with one another, as shown for the two shallower peaks in Fig. 2a at 90 min and in Fig. 2b at 0.1 day. The isolated plateau concentration is denoted $C_{\mathrm{mid}i}$, and is given by

$$C_{\mathrm{mid}i} = \frac{q_i(C_i - C_0)}{\sum q_j} + C_0 \tag{9}$$

where the denominator sum runs over all $z_j \geqq z_i$. Eq. (9) is derived from Eq. (4) by replacing C_j with C_0 for the $z_j > z_i$ peaks. As before, Eq. (9) may be solved for q_i and Eq. (6) used to determine C_i, enabling determination of q_i and C_i for the ith peak, given $C_{\mathrm{mid}i}$ and the $q_i(C_i-C_0)$ products for the ith and all deeper peaks. Note that for the lowest peak, $C_{\mathrm{mid}1} = C_{\mathrm{max}1} = C_1$. If some peaks interfere and others do not, then Eq. (5) should be used to determine q_i, with C_j replaced by C_0 for non-interfering peaks.

Upflow from below the wellbore section being investigated can occur when the bottom of the section is not sealed with a packer. If the upflow from below has a distinctive salinity, it can simply be treated as another inflow point, but if it has salinity C_0, it will not exhibit a peak of its own and its presence must be inferred from its influence on the other peaks. The addition of upflow from below causes all peaks to become more strongly skewed upward. The most evident change occurs at the lower limb of the lowest peak, which shows a dispersive profile with no upflow and a combination of advection and dispersion when upflow is present. Integration under the early-time $C(z)$ peaks provides $q_i(C_i-C_0)$ estimates as before, despite the asymmetric shape of peaks, but, since the peaks interfere sooner, care must be exercised in choosing the extent of integration. The steady-state mixing rules (Eqs. (3)–(6)) must be modified when upflow is present (Doughty and Tsang, 2002), and in general it is not possible to determine all feed point properties individually.

2.1.2. Time-dependent feed points

Time-dependent values of q_i and C_i most commonly arise when pumping rates are altered during logging or tracers are introduced in nearby wells. However, they can also represent actual physical or chemical variations in the formation liquid near the borehole. Fig. 3 shows the concentration profiles simulated by BORE II for a single inflow point in which feed-point concentration is either constant at C_1 (Fig. 3a), increases linearly from 0 to C_1 (Fig. 3b), or decreases linearly from C_1 to 0 (Fig. 3c and d). A decreasing feed-point concentration provides a distinctive concentration profile signature, particularly when combined with upflow. In contrast, the profiles for increasing feed-point concentration or increasing feed-point inflow rate (not shown) may be difficult to distinguish from those for a constant feed point. For early times, before the profiles for adjacent inflow points begin to interfere with each other, Eq. (1) for $M_i(t)$ can be generalized to obtain

$$M_i(t) = \int_0^t q_i(t')(C_i(t') - C_0)\,\mathrm{d}t', \tag{10}$$

where t' is a dummy integration variable. The slope of the $M_i(t)$ versus t curve gives $q_i(t)(C_i(t)-C_0)$. This approach does not distinguish between time dependencies in q_i or C_i, but the skewness of concentration peaks, which depends only on q_i, may provide insight into q_i and C_i time variations. If either q_i or C_i is known to be constant, then Eq. (10) can be used to calculate the time dependence of the other quantity.

A common concentration time dependence, which arises if de-ionized water migrates into the fracture during the replacement of borehole water prior to wellbore logging, is C_i constant after a time t_{0i}, but $C_i = C_0$ before t_{0i}. In this case, it is generally possible to estimate t_{0i} along with $q_i(C_i-C_0)$ by integrating over a series of profiles and fitting the resulting $M_i(t)$ values to the linear relation

$$M_i(t) = q_i(C_i - C_0)(t - t_{0i}). \tag{11}$$

2.1.3. Inflow points with $C_i = C_0$

It may happen that the initial wellbore ion concentration C_0 is similar to some of the feed point concentrations, i e. for some feed points, $C_i = C_0$. An inflow point with $C_i = C_0$ does not show a concentration peak of its own, but its effect on neighboring

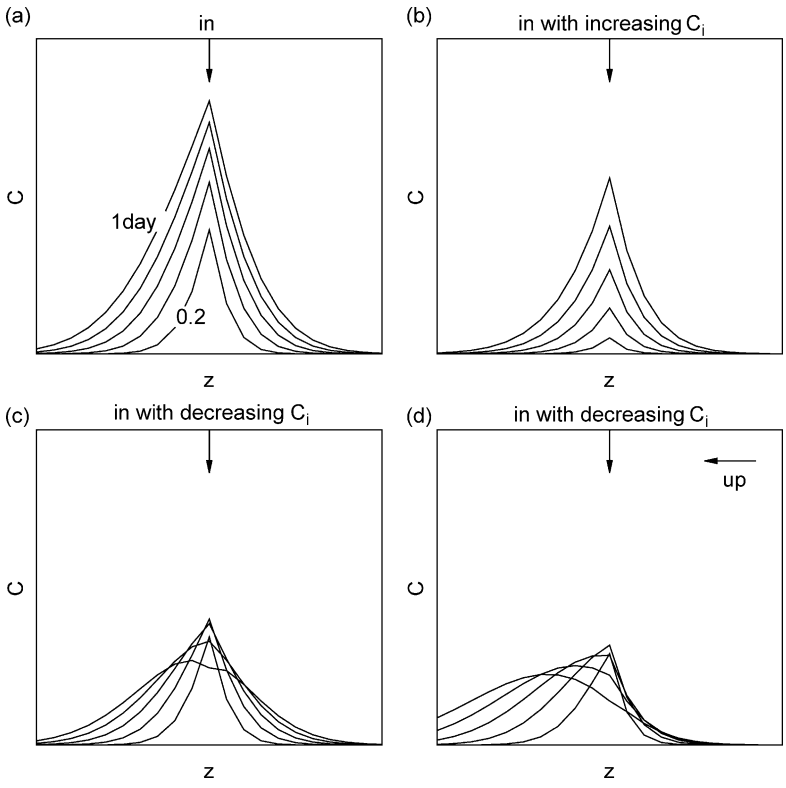

Fig. 3. Simulated concentration profiles obtained at early times for inflow points with (a) constant C_i; (b) increasing C_i; (c) decreasing C_i; and (d) decreasing C_i and upflow from below. The profiles are equally spaced in time.

peaks may be visible. Fig. 4 shows the concentration profiles simulated by BORE II for two inflow points, one of which has $C_i = C_0 = 0$. In each of the four examples in Fig. 4, the inflow rate of the $C_i = C_0$ inflow point is twice that of the adjacent inflow point. If the $C_i = C_0$ inflow point is above (down-gradient of) the other inflow point, there is a subtle signature in the form of a break in slope of the concentration profiles when the diluting effect of the $C_i = C_0$ inflow is first observed (Fig. 4a). This break in slope is accentuated if upflow from below is present (Fig. 4b). At late times, the $C_i = C_0$ inflow point causes a distinctive plateau (Fig. 4c). If the $C_i = C_0$ inflow is below (up-gradient of) the other inflow point, the break in slope is difficult to see (Fig. 4d). The concentration profile is skewed upward as when upflow from below is present, suggesting the presence of a $C_i = C_0$ inflow, but not its location.

2.1.4. Outflow points

Simultaneous outflow and inflow from different feed points may occur when the far-field hydraulic head conditions for the individual conducting fractures and permeable zones penetrated by the wellbore are different. When the well is shut in or is pumped at very low rates, groundwater flows into the wellbore from the higher head zone, is transmitted through the wellbore, and flows out into a lower-head zone. This process is known as internal wellbore flow. Fig. 5 shows the concentration profiles simulated by BORE II for an outflow point located adjacent to an inflow point. In each example, the outflow strength is twice the inflow strength. The outflow points cause subtle changes in the shape of the peaks, but these changes do not identify the outflow location clearly. The addition of upflow from below changes the peak shape, but does not help identify the outflow location.

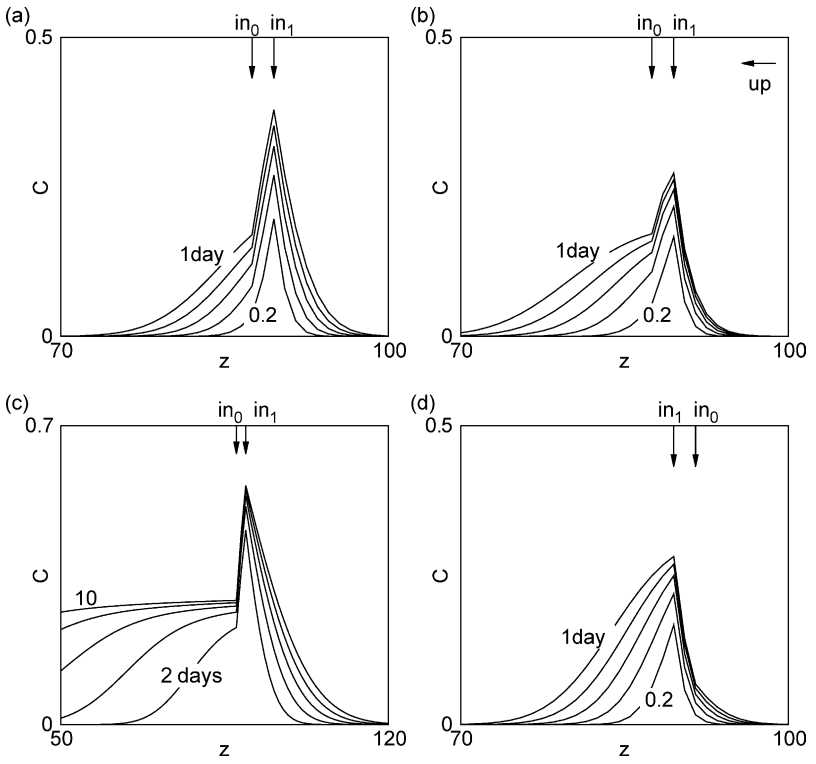

Fig. 4. Simulated concentration profiles for an inflow point with $C_i = C_0 = 0$ (labeled in_0) and another inflow point (labeled in_1): (a) in_0 above in_1; (b) in_0 above in_1 with upflow from below; (c) in_0 above in_1 at long times; and (d) in_0 below in_1. In each case, in_0 has double the strength of in_1. The profiles are equally spaced in time.

An integral method that can be used to estimate the outflow location is presented in the Section 2.2.

Fig. 6 shows a special situation where the $C(z)$ profiles themselves can provide information on outflow point location and strength. The figure shows the concentration profiles simulated by BORE II for well-separated inflow and outflow points, with profiles collected frequently enough to quantify the speed at which the concentration front moves up the wellbore. By examining the spacing between concentration profiles obtained at known time intervals, the location and strength of the outflow point can be inferred. In this case, the speed of the front is halved as it passes the outflow point, indicating that $q_{out} = (q_{in} + q_{up})/2$.

2.1.5. Horizontal flow

Horizontal flow across the wellbore may be used to estimate the natural regional flow in a hydrologic layer (Drost et al., 1968) and can be investigated by flowing FEC logging with a very small or zero pumping rate. In BORE II, horizontal flow can be represented with a pair of inflow and outflow feed points located at the same depth, with $q_1 \equiv q_{in} = Q_0$ and $q_2 \equiv q_{out} = -Q_0$, where Q_0 is the volumetric flow rate across the wellbore. Q_0 can be related to the regional Darcy velocity v_d in the layer intercepted by the wellbore using $Q_0 = v_d 2rb\alpha_h$, where r is the wellbore radius, b is the thickness of the hydrologic layer, and α_h is a dimensionless convergence factor ranging from 1 to 4, which depends on well completion (Drost et al., 1968). At early times, the concentration profiles for inflow and horizontal flow are similar, both showing symmetric profiles. At later times, the horizontal-flow profiles remain symmetric, whereas the inflow profiles become skewed up the wellbore. Peak concentration increases faster with inflow only, but in the absence of longitudinal dispersion, the steady-state concentration C_{max} would be $C_1 \equiv C_{in}$ for both cases.

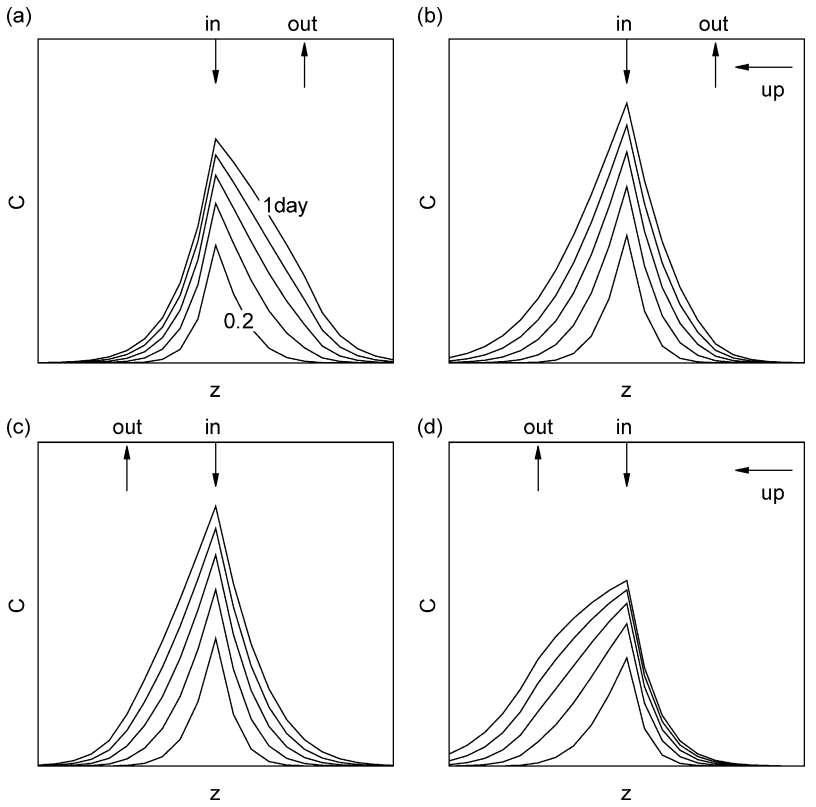

Fig. 5. Simulated concentration profiles obtained at early times for an outflow point (a) below an inflow point; (b) below an inflow point with upflow from below; (c) above an inflow point; and (d) above an inflow point with upflow from below. In each case, the outflow point has double the strength of the inflow point. The profiles are equally spaced in time.

In the field, dispersion along the wellbore is typically too strong to be neglected. Thus, C_{max} for a thin layer of horizontal flow is likely to be much less than C_{in} (Fig. 7a). However, for thick layers of horizontal flow, dispersion has little impact at the center of the flow layer, allowing the concentration profiles to reach $C_{max} = C_{in}$ (Fig. 7b). The black dots on the horizontal-flow profiles in Fig. 7b show the concentration given by an analytical solution (Drost et al., 1968) that considers horizontal flow only (i.e. longitudinal diffusion and dispersion are negligible or the hydrologic flow layer is very thick):

$$C(t) = C_{in} - [C_{in} - C_0]\exp\left(\frac{-2tv_d\alpha_h}{\pi r}\right). \qquad (12)$$

The BORE II simulation of a thick horizontal-flow layer matches the analytical solution well. Fig. 8 shows $C(t)/C_{in}$ at the center of the flow layer as

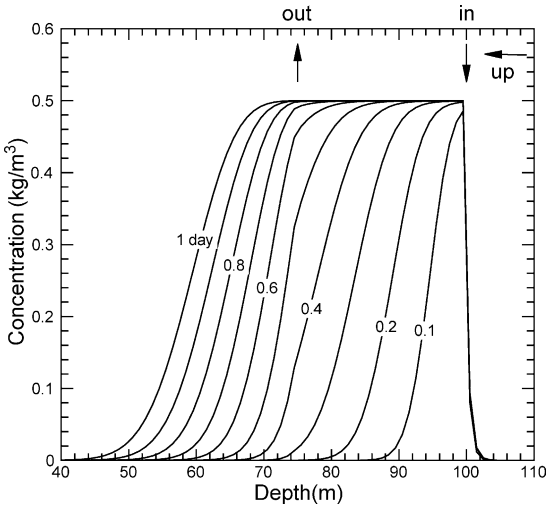

Fig. 6. Simulated concentration profiles obtained at long times for widely separated inflow and outflow points.

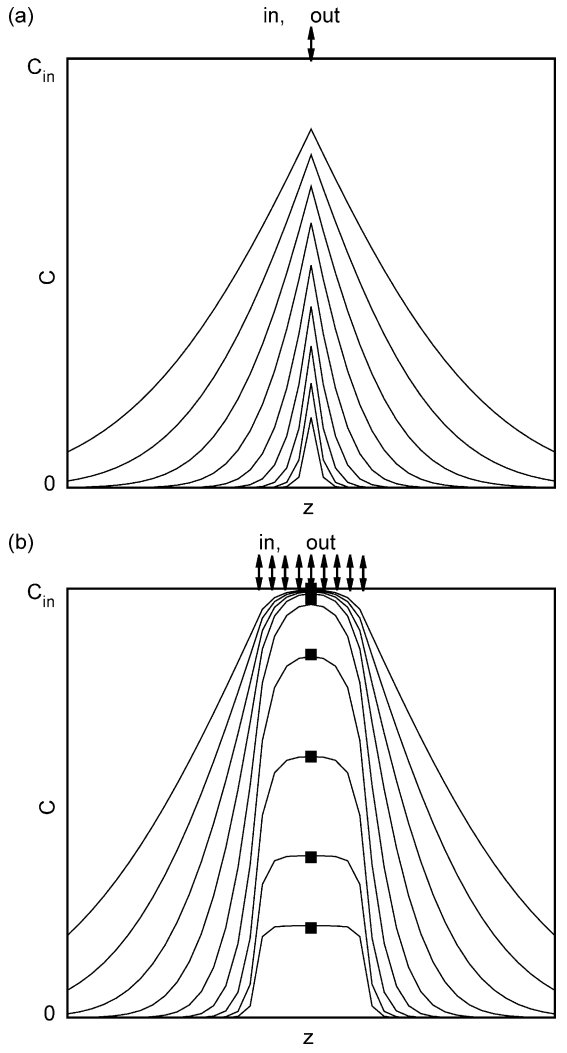

Fig. 7. Simulated concentration profiles for (a) a thin layer of horizontal flow; and (b) a thick layer of horizontal flow (the Drost et al. (1968) analytical solution is shown as symbols). The time interval doubles between successive concentration profiles.

a function of time for thin and thick layers of horizontal flow with large and small values of D_0, and the Drost et al. (1968) solution. Both thick-layer BORE II simulations follow the analytical solution closely, regardless of the value of D_0 applied, and the thin-layer case with small D_0 shows similar behavior. However, for a thin layer (such as a narrow conducting zone or a single fracture) with a large (i.e. more realistic) value of D_0, the peak concentration grows much more slowly. Dispersion plays

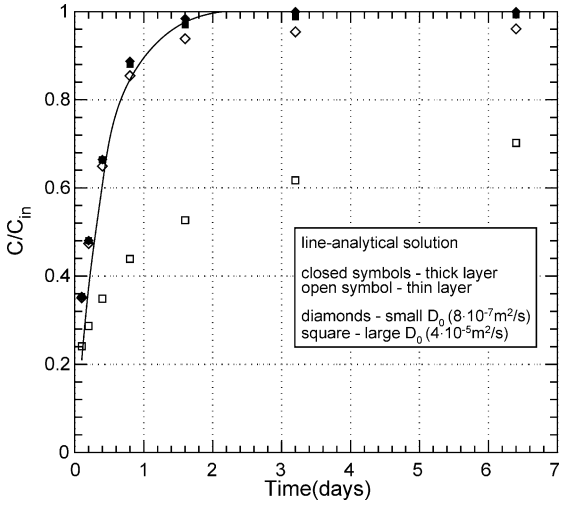

Fig. 8. Simulated concentration versus time curves for several horizontal-flow cases and the Drost et al. (1968) analytical solution.

a significant role, decreasing the concentration at the feed-point by effectively mixing formation water with wellbore water. In this case, matching with BORE II will yield a more accurate estimate of horizontal flow than Drost's solution.

2.2. Mass integrals

The examples of concentration profiles shown in the previous section indicate that in general, outflow points do not produce a strong signature that enables them to be easily located Here, we describe an integral procedure that enables outflow points to be located by examining changes in ion mass in the wellbore section.

Consider a wellbore section with one or more outflow points above one or more inflow points, and assume feed-point strength and concentration do not vary in time. The procedure is as follows. Each $C(z)$ profile is integrated over the entire wellbore section of interest to obtain the area $A(t)$ under the $C(z)$ profile at time t (including all peaks, whether or not they interfere). Then, $A(t)$ is multiplied by the mean wellbore cross-sectional area to determine ion mass in place at time t, which is denoted the mass integral $M(t)$. Then $M(t)$ is plotted versus t. Note that before the concentration front reaches any outflow points,

$M(t)$ is linear, with slope

$$S_{\text{early}} = \sum_{\text{in}} q_i(C_i - C_0). \tag{13}$$

When the concentration front reaches an outflow point, the slope of $M(t)$ decreases, since ion mass leaves the wellbore at that point. When the concentration front passes the uppermost outflow point, $M(t)$ becomes linear again, with slope

$$S_{\text{late}} = \sum_{\text{in}} q_i(C_i - C_0) - \sum_{\text{out}} q_i(C_{\text{max}i} - C_0). \tag{14}$$

Since all outflow points are above all inflow points and steady-state concentration does not change at outflow points, all outflow $C_{\text{max}i}$ values are the same and equal the steady-state concentration at the uppermost inflow point, which is denoted C_{max}. Thus Eq. (14) simplifies to

$$S_{\text{late}} = S_{\text{early}} - (C_{\text{max}} - C_0) \sum_{\text{out}} q_i. \tag{15}$$

To determine the aggregate outflow rate, Eq. (15) is rearranged to yield

$$\sum_{\text{out}} q_i = \frac{S_{\text{early}} - S_{\text{late}}}{C_{\text{max}} - C_0}. \tag{16}$$

Next, the $C(z)$ profiles are examined to locate the times when (a) $M(t)$ becomes nonlinear and (b) $M(t)$ becomes linear again. The leading edge of the concentration front at (a) identifies the deepest outflow point, z_{max}. The trailing edge of the concentration front at (b) identifies the shallowest outflow point, z_{min}. Here, we somewhat arbitrarily define the leading edge as the z location at which $C(z) = 0.1C_{\text{max}}$ and the trailing edge as the z location at which $C(z) = 0.9C_{\text{max}}$. The validity of these definitions will be tested in the application of the method.

An example of the mass-integral procedure for early-time concentration profiles is shown in Fig. 9. A single inflow point is located below a single outflow point in a wellbore section with upflow from below. The concentration profiles simulated by BORE II (Fig. 9a) contain a minor break in slope at the outflow point, which would probably be impossible to identify in actual log data. In contrast, the mass-integral plot (Fig. 9b) shows a clear divergence from linearity between $t = 0.4$ and $t = 0.6$ days. The $C(z)$ profiles indicate that the leading edges of the $t = 0.4$-day and

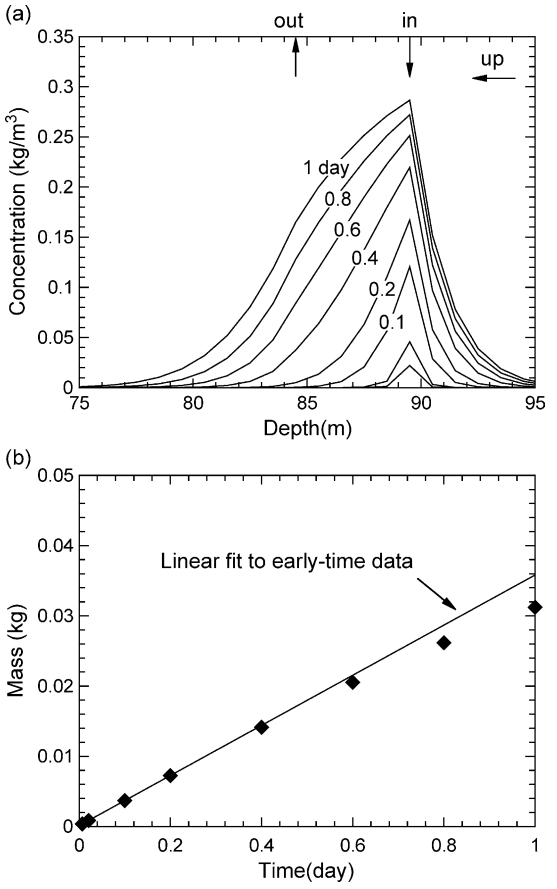

Fig. 9. Short-time example of the mass-integral method: (a) simulated concentration profiles; and (b) $M(t)$ integral and linear fit to early points.

$t = 0.6$-day profiles are at $z = 84$ and $z = 82.5$ m, respectively. Since the $t = 0.4$-day integral fits the linear $M(t)$ trend but the $t = 0.6$-day integral does not, the outflow point is inferred to be in the range $82.5 \le z \le 84$ m. The actual location specified for the outflow point is 84.5 m. Hence the $M(t)$ method, while not perfect, does provide useful information for outflow-point location.

Another example, considering longer-time concentration profiles, is shown in Fig. 10. Two inflow points are located below two outflow points in a wellbore section with upflow from below. The concentration profiles simulated by BORE II (Fig. 10a) show interference between two inflow peaks, which makes it difficult to simply locate the outflow points by

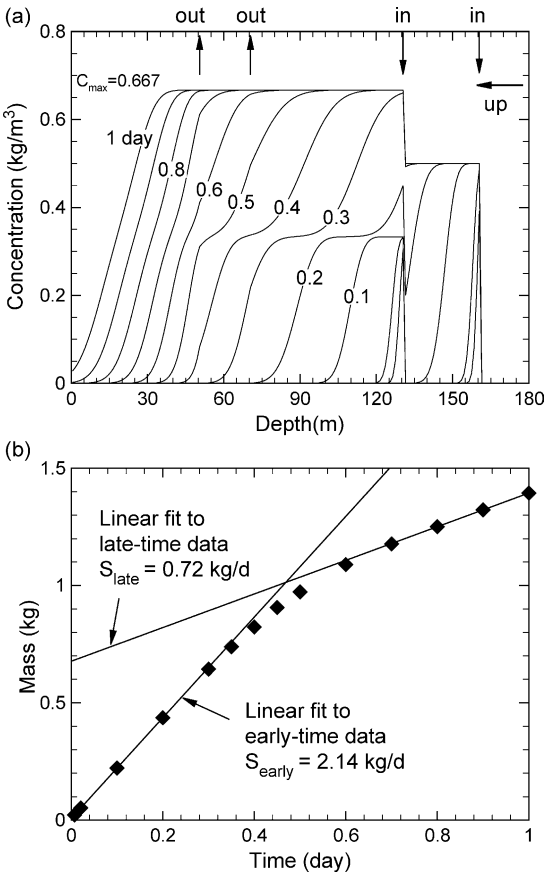

Fig. 10. Long-time example of the mass-integral method: (a) simulated concentration profiles; and (b) $M(t)$ integral and linear fits to early and late points.

inspection. The mass-integral plot (Fig. 10b) shows early-time and late-time linear sections, with a departure from linearity for $t=0.3$ days and a return to linearity by $t=0.7$ days. The leading edge of the $t=$ 0.3-day profile is at $z=65$ m, suggesting that the deepest outflow point is just below this depth. The trailing edge of the $t=0.7$-day profile is at $z=50$ m, suggesting that the shallowest outflow point is just below this depth. These predictions are reasonably close to the actual locations specified for the outflow points (70.5 and 50.5 m). Using Eq. (16) with the values of S_{early}, S_{late}, and C_{max} shown in Fig. 10 yields an aggregate outflow rate of 1.48 L/min, which agrees closely with the actual value, 1.5 L/min.

Note that in theory, if two outflow points are separated by a large enough distance, a linear portion in the $M(t)$ plot will develop when the concentration fronts are between the two points, potentially enabling the locations and strengths of the individual points to be determined. However, if the two points are separated by a distance comparable to or less than the width of the concentration fronts, as in Fig. 10, the $M(t)$ method will not be able to resolve them.

3. Effect of pumping rate

Feed-point analysis can be expedited by comparing sets of FEC logs obtained with different pumping rates. Fig. 11 shows how $C(z)$ and $M(t)$ depend on pumping rate Q for an example containing both inflow and outflow points. For the original Q value (Fig. 11a), the outflow point produces only a subtle change in slope in the $M(t)$ plot, making the mass-integral procedure difficult. If Q is halved (Fig. 11b), the change in slope becomes larger and the analysis becomes easier. On the other hand, if Q is doubled (Fig. 11c), the outflow point becomes an inflow point and is easily identified in the early-time $C(z)$ profiles as another peak. Finally, if Q is reduced to zero (Fig. 11d), corresponding to a shut-in well with internal wellbore flow, then the outflow point captures all the flow in the wellbore. In this case, the $C(z)$ profiles would provide a strong signature of the outflow point. Because one does not know a priori what value of Q will produce the most striking signatures in the $C(z)$ profiles or $M(t)$ curves, it is valuable to repeat the logging process with several different values of Q.

Additionally, repeated logging runs with different Q values, a procedure known as multi-rate flowing FEC logging, may be used to obtain additional information on each feed point, namely the transmissivity and far-field pressure head of the conductive feature represented by the feed point. A quantitative relationship between the change in feed-point strength Δq_i with a change in pumping rate ΔQ, derived in Tsang and Doughty (2003), provides the basis for this study. Here, we just describe the assumptions made for the analysis and quote the final results, then focus on the signatures produced by multi-rate flowing FEC logging.

Consider a wellbore interval containing N feed points, being pumped at a rate Q. The strength of

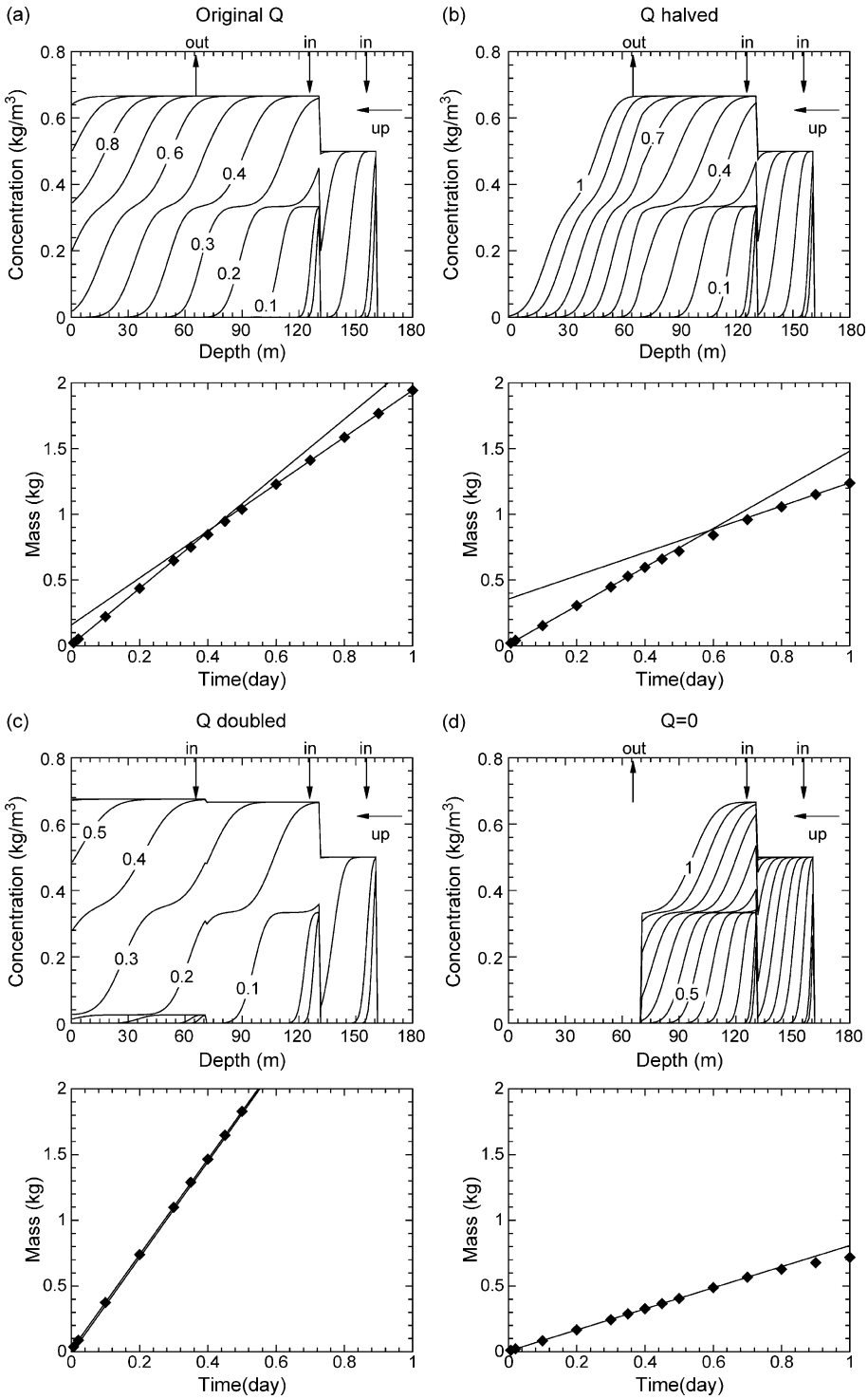

Fig. 11. The effect of varying Q on concentration profiles and mass integral for an example containing inflow and outflow points.

the ith feed point is q_i and it is assumed that $\Sigma q_i = Q$. By convention, inflow points have positive q_i and outflow points have negative q_i. For each feed point, q_i and concentration C_i are assumed to be constant in time. Further, flow toward the well is assumed to obey Darcy's Law and the flow geometry is assumed to be the same for all flow zones (but not necessarily radial). Under these assumptions, the strength of a feed point q_i is related to its hydraulic transmissivity T_i, the ambient 'far-field' pressure head h_i, and the pressure head h_{wb} at the wellbore radius. The vertical hydraulic transmissivity of the wellbore itself is typically much greater than that of any inflow zone, so that h_{wb} is constant over the wellbore interval of interest. Suppose that two sets of flowing FEC logs were measured, using Q_1 and Q_2, with $Q_2 - Q_1 \equiv \Delta Q$, and that the resulting BORE II analyses yielded $q_i^{(1)}$ and $q_i^{(2)}$, with $q_i^{(2)} - q_i^{(1)} \equiv \Delta q_i$. Then a simple derivation (Tsang and Doughty, 2003) yields

$$\frac{T_i}{T_{tot}} = \frac{\Delta q_i}{\Delta Q} \tag{17}$$

$$\frac{(h_i - h_{avg})}{(h_{avg} - h_{wb}^{(1)})} = \frac{q_i^{(1)}/Q_1}{\Delta q_i/\Delta Q} - 1 \tag{18}$$

where $T_{tot} = \Sigma T_i$ can be obtained by a normal well test over the whole length of the borehole, $h_{avg} = \sum(T_i h_i)/T_{tot}$ is the steady-state pressure head in the borehole when it is shut in for an extended time, and $h_{wb}^{(1)}$ is the pressure head in the wellbore during the logging conducted while $Q = Q_1$. Eq. (17) is the fundamental relationship between the change in feed-point strength Δq_i and the change in pumping rate ΔQ. Note that Δq_i is directly proportional to T_i, and thus the feed points with larger hydraulic transmissivity show greater changes in strength when Q is modified. The dimensionless group on the left-hand-side of Eq. (18) provides a measure of h_i for each feed point. However, it depends on pumping rate Q_1 through the parameter $h_{wb}^{(1)}$. This Q dependence becomes inconvenient if several pairs of tests using different values of Q are to be compared. Hence, both sides of Eq. (18) are multiplied by Q_1

$$\frac{(h_i - h_{avg})}{(h_{avg} - h_{wb}^{(1)})} Q_1 = \left(\frac{q_i^{(1)}/Q_1}{\Delta q_i/\Delta Q} - 1 \right) Q_1. \tag{19}$$

The ratio $Q_1/(h_{avg} - h_{wb}^{(1)})$ is known in the petroleum literature as the productivity index I, defined as the ratio of pumping rate to drawdown during a well test. I characterizes the well and the permeable formation it intersects, but is independent of Q. Defining $(h_i - h_{avg}) = \Delta h_i$, Eq. (19) becomes

$$I \Delta h_i = \left(\frac{q_i^{(1)}/Q_1}{\Delta q_i/\Delta Q} - 1 \right) Q_1 \tag{20}$$

The quantity $I\Delta h_i$, provides a measure of inherent pressure head for the ith feed point that is independent of Q.

There are several special cases of Eq. (17) that are of interest. If all the T_i's are the same, then $T_i = T_{tot}/N$, and Eq. (17) simplifies to

$$\Delta q_i = \frac{\Delta Q}{N}, \tag{21}$$

where N is the number of feed points. In this case, when Q is modified, all feed-point strengths change by the same amount.

On the other hand, if the h_i's are all the same ($h_i = h_{avg}$), then Eq. (18) simplifies to

$$\frac{\Delta q_i}{q_i^{(1)}} = \frac{\Delta Q}{Q_1}. \tag{22}$$

In this case, when Q_I is modified, the relative change of each feed point $\Delta q_i/q_i$ is the same and is equal to the relative change of $Q_{'1}$. Conversely, increasing or decreasing Q_1 by a factor of two and finding $q_i^{(1)}$ not changed by the same factor of two is a clear indication that the h_i's are not the same.

Fig. 12 shows how changes in q_i resulting from a change in Q provide information on T_i and h_i for various feed points. Fig. 12a shows feed point strengths q_i for a synthetic data set consisting of ten feed points, for two different Q values. Fig. 12b and c show Δq_i and $\Delta q_i/q_i$, respectively, for each feed point. According to Eq. (17), feed points with the same values of T_i yield the same values of Δq_i, as shown in Fig. 12b. According to Eq. (18), feed points with the same values of h_i yield the same values of $\Delta q_i/q_i$, as shown in Fig. 12c. This analysis is particularly valuable for identifying flow compartmentalization, because flow zones that are hydraulically isolated from one another can develop distinct hydraulic head values.

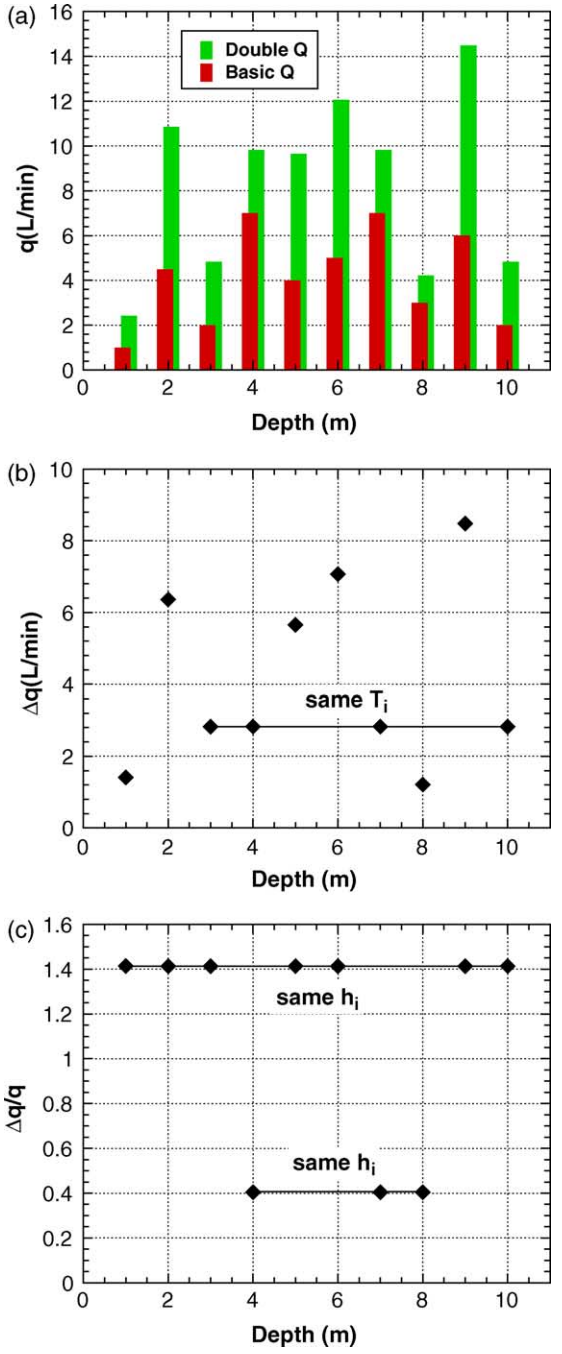

Fig. 12. The effect of varying Q on inflow rates q_i: (a) inflow rates for base Q and doubled Q; (b) Δq for each feed point (feed points with the same Δq_i have the same T_i); (c) $\Delta q/q$ for each feed point (feed points with the same $\Delta q/q$ have the same h_i).

4. Application to two field cases

4.1. Raymond field site

At the Raymond field site, located in the foothills of the Sierra Nevada Mountains in California, nine wells were drilled into a fractured granodiorite. The wells are 90 m deep and are cased only over the upper 8 m through a sediment layer. A variety of well logs and well tests have been conducted in these wells, for the purpose of developing and testing equipment and methodologies for characterizing the hydrological behavior of fractured rock (Karasaki et al., 2000). Flowing FEC logging was carried out in seven of the nine wells (Cohen, 1995) using pumping rates ranging from 7 to 20 L/min. Six or seven downward logging profiles were obtained for each well. Because the wells are quite shallow, borehole temperatures do not vary much with depth, and FEC values do not need to be corrected for temperature variations (see Appendix A). FEC is converted to C using the quadratic relationship given in Eq. (A1). Below, we present and analyze concentration profiles from one of the wells at the Raymond site.

Fig. 13 shows the concentration profiles for well SW1. Six peaks can be identified. The dispersive

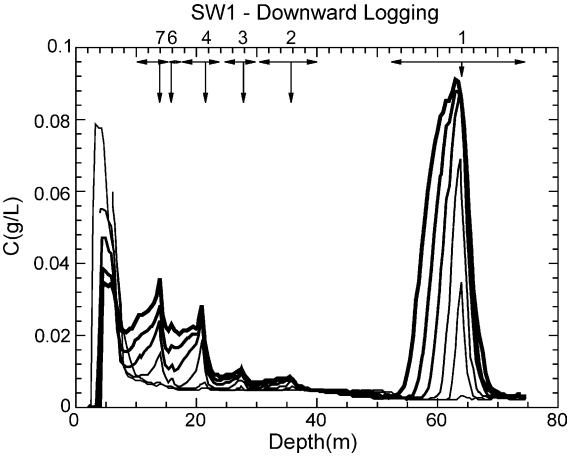

Fig. 13. Concentration profiles obtained from flowing FEC logging of well SW1 at the Raymond field site in California (K. Karasaki, personal communication, 2001; see also Karasaki et al., 2000). Concentration profile times (in minutes) are 1.8, 14, 25, 39, 52, and 66, with later profiles shown as thicker lines. The vertical arrows identify feed-point locations and the horizontal arrows indicate the integration range for the corresponding peak.

shape of the lower limb of the lowest peak (peak 1) suggests that there is no upflow from below. Most peaks show an approach to steady state, enabling estimates of C_{maxi} to be made. The shallowest peak (z=2–8 m), which decays rather than grows, is not analyzed on the assumption that it is evidence of leakage around the casing rather than inflow from a hydraulically transmissive zone. Such leakage has been confirmed for most of the wells by field observations (Cohen, 1995). A constant value of C_0=0.0048 g/L is assumed. Some of the peaks are well enough separated to enable the use of the area under the individual peaks to determine $M_i(t)$, the mass arising from the ith feed point as a function of time (Fig. 14). Straight line fits to $M_i(t)$ and Eq. (11) identify the slopes of the lines as $q_i(C_i-C_0)$ and the time-axis intercepts as t_{0i}. In general, the late-time drop in $M_i(t)$ below the linear fitting line does not identify outflow, as described in Section 2, but indicates the peak reaching the edge of the integration domain. Note that in Fig. 13, peak 6 overlaps with surrounding peaks too early for the estimates of $q_6(C_6-C_0)$ and t_{06} from $M_6(t)$ to be reliable.

For peak 1, the $q_1(C_1-C_0)$ product is well defined, but there is no evidence of a C_{max1} plateau. Furthermore, the height of an isolated peak such as this is very sensitive to diffusion/dispersion strength D_0, which is unknown. Therefore, we search for D_0 as well as q_1 and C_1 values by trial and error using the BORE II code, by comparing the observed $C(z)$ profiles for peak 1 to simulation results. The two main attributes of the peak to be matched are the skewness and the height. With the $q_1(C_1-C_0)$ product known, there are two independent unknowns, making the inverse problem well posed.

Once C_1 and q_1 have been found, Eqs. (5) and (6) can be used to calculate the parameters of the upper peaks. Because peak 1 does not interfere with the upper peaks, C_1 is replaced by C_0 in Eq. (5). The upper portion of Table 2 summarizes the results. Note that inflow point 5 has $C_5=C_0$, to account for the narrow peak 4 and lower plateau above it (compare to Fig. 4). Unfortunately, the shallow leakage around the casing precludes the use of Q to constrain the q_i values. Fig. 15a shows $C(z)$ profiles simulated with BORE II using the parameters given in the upper portion of Table 2. The simulated profiles match the observed ones approximately, but there is room for improvement. In particular, peak 6 is much too small and there is generally not enough interference between the upper four peaks. Because the peaks overlap relatively early, the $M_i(t)$ integrals cannot extend as far along the wellbore as they should. Thus, the integrals tend to underestimate the $q_i(C_i-C_0)$ products, which in turn leads to too-small values of q_i.

The q_i and C_i values shown in the upper portion of Table 2 are then optimized by data fitting using BORE II simulations. Fig. 15b shows the results of this fitting process, and the lower portion of Table 2 shows the corresponding feed-point properties. Overall, the property changes required for the existing feed points are minor. Peaks 5–7 require more adjustment than peaks 1–4, but examination of the $C(z)$ profiles (Fig. 13) made it clear a priori that the upper peaks were too close together for the individual-peak integration to be reliable. These flowing FEC logging results for well SW1 are typical of results obtained for all the wells at the Raymond site.

It is interesting to note the advantages of the flowing FEC logging method at this particular site. From one set of data, obtained in only about one hour (Cohen, 1995), seven conducting fractures are identified intersecting the well. Table 2 shows that the salinity of water from the seven inflow points varies by a factor of two, except for one point that has very low salinity, and that the variation of feed point flow rate q_i covers a range of almost two orders of magnitude. If all the h_i's are assumed to be the same, the hydraulic transmissivities of the flowing fractures T_i can be calculated directly from the flow rates q_i, by combining Eqs. (17) and (22), with T_{tot} obtained from an open-hole pump test and taking $Q=\Sigma q_i$. Results are shown in the final row of Table 2 and Fig. 16. Consistent transmissivity information was obtained using conventional packer tests (Cohen, 1995), requiring considerable more time and effort with much less spatial resolution along the well.

Fig. 16 also compares the q_i values shown in the lower portion of Table 2 with measurements made with a downhole flow meter (Cohen, 1995). The downhole flow meter, packer tests, and flowing FEC logging all provide consistent results, supporting the conceptual flow model developed for the Raymond

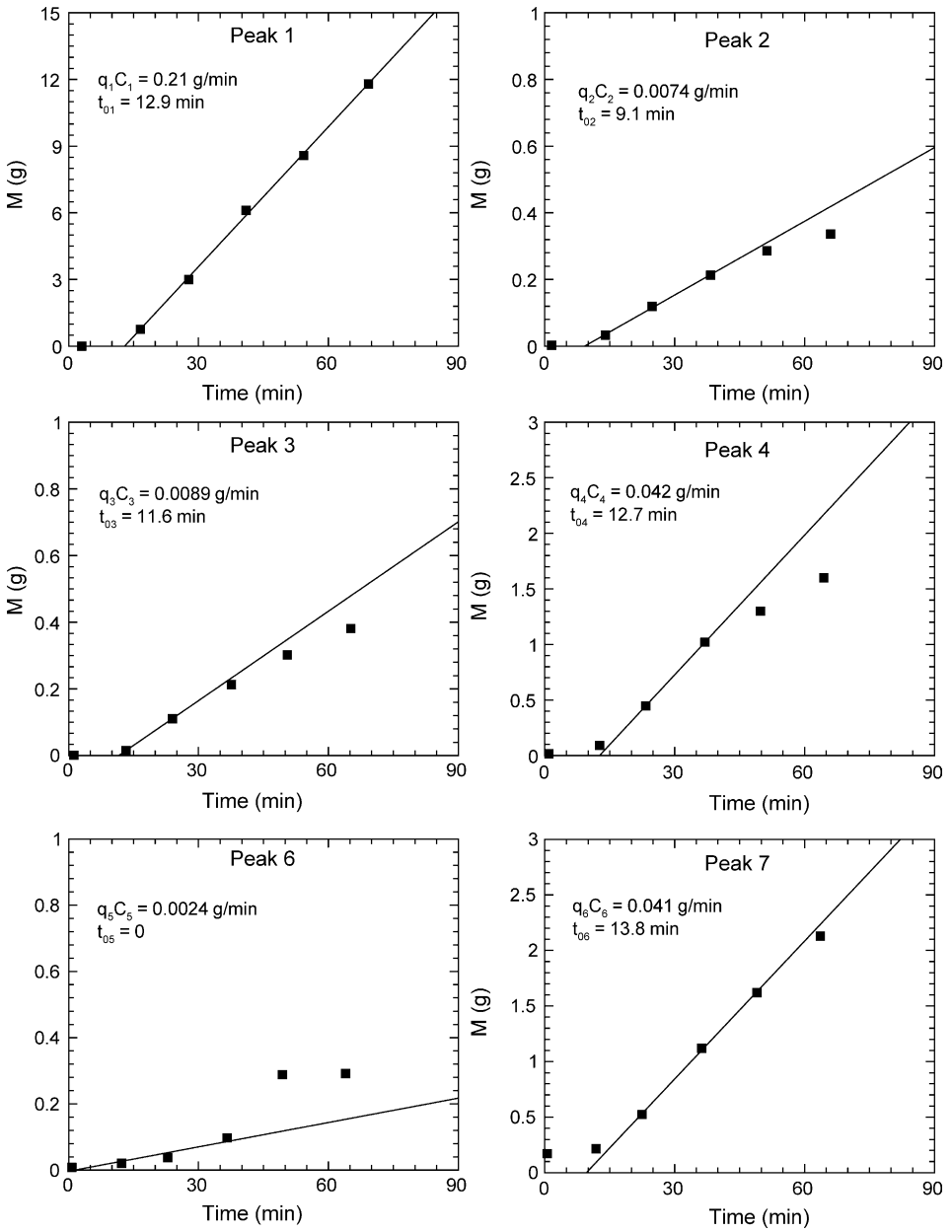

Fig. 14. Mass integrals $M_i(t)$ for the six concentration peaks shown in Fig. 13 and the linear fits used to determine $q_i(C_i - C_0)$ (slope) and t_{0i} (time-axis intercept).

site of two sub-horizontal fracture zones (10–40 and 60–80 m depth) separated by lower permeability rock (Karasaki et al., 2000). Note that the spatial resolution of the downhole flow meter varies greatly: the high-resolution series of measurements between depths of 20 and 30 m requires repeated deflation, movement, and re-inflation of the packers isolating the flow meter, whereas the low-resolution measurements for the 9–21 and 65–75 m depth intervals do a poor job of locating transmissive fractures.

Table 2
Parameters estimated for Raymond well SW1 using analysis of concentration profile signatures (corresponding $C(z)$ profiles are shown in Fig. 15a) and trial and error BORE II analysis (corresponding $C(z)$ profiles are shown in Fig. 15b)

	Parameter	How determined	Feed point						
			1	2	3	4	5	6	7
Signature analysis	z (m)	Observed from early-time $C(z)$ profiles	64	36	28	22	20	16	14
	$q(C-C_o)$ (g/min)	Calculated from area under early-time $C(z)$ peak	0.21	0.007	0.009	0.042	0	0.002	0.041
	C_{max} (g/L)	Estimated from late-time $C(z)$ profiles	0.11[a]	0.008	0.012	0.029	0.023	0.024	0.035
	q (L/min)	Calculated from current C_{max} and current and deeper $q(C-C_0)$ values (Eq. (5))	2.1[a]	0.058	0.062	0.21	0.77	0.045	0.13
	C (g/L)	Calculated from $q(C-C_0)$ and q values (Eq. (6))	0.11[a]	0.13	0.15	0.21	0.005	0.059	0.32
Bore II analysis	q (L/min)	Trial and error	2.1	0.058	0.070	0.25	0.60	0.057	0.20
	C (g/L)	Trial and error	0.11	0.13	0.15	0.21	0.005	0.22	0.24
	T_i (10^{-6} m^2/s)	Proportional to q_i if all h_i assumed to be the same[b]	13	0.35	0.42	1.5	3.6	0.34	1.2

[a] Determined by trial and error using BORE II.
[b] Uses $T_{tot}=2\times10^{-5}$ m^2/s obtained from an open-hole pump test (Cohen, 1993).

4.2. Colog field site

The flowing FEC logs shown in Fig 1 are proprietary and the site geologic information is not made known to us. Nevertheless they provide a good example of using the mass-integral method to identify the location and strength of an outflow point. The FEC logs are converted to concentration profiles using Eq. (A1). Fig. 17a shows the $C(z)$ profiles for a series of 12 times, and Fig. 17b shows the corresponding $M(t)$ integral for the entire wellbore section from $z=146$ to $z=226$ m. The first two points on the $M(t)$ curve essentially represent the initial conditions, so they are not included in the early-time data fit to a straight line, which yields $S_{early}=0.081$ kg/h and $t_0=0.22$ h. The initial deviation from linearity occurs at a time $t=1.6$ h. According to Fig. 17a, the concentration front at this time is at a depth of $z=212$ m, which is inferred to be the outflow-point location, denoted z_{out}. Fitting the subsequent data to a straight line yields $S_{late}=0.059$ kg/h. Note that after a time of $t=2.6$ h, the concentration profiles do not show complete peaks, so subsequent points are not included in the fit. Setting the C_{max} value at $t=2.6$ h as 0.69 kg/m^3 in Eq. (16), an outflow strength $q_{out}=0.029$ m^3/h$=$ 0.49 L/min is obtained. An alternative procedure to determine q_{out}, which involves correcting the $M(t)$ integral to account for the fact that the limits of integration do not include entire concentration peaks (Tsang et al., 1990; Doughty and Tsang, 2002), provides similar outflow strength.

Analysis of the remaining features of the $C(z)$ profiles shown in Fig. 1 (multiple inflow points, including an inflow point with $C=C_0$, downflow out the bottom of the logged wellbore section, and a non-uniform initial condition), as well as a numerical analysis with BORE II, are presented elsewhere (Doughty and Tsang, 2000).

5. Summary and conclusions

Flowing FEC logging is a practical method for hydrologic characterization of individual fractures, fracture zones, or permeable layers intersecting a borehole. This paper explores the analysis of complex FEC logs to identify and interpret signatures of various flow conditions. This can greatly expedite setting up the numerical model of the borehole/fracture system used to simulate conductivity logging and provides a sound basis for development of an automatic inversion method. For each feed point along the borehole, location, flow rate, and (for inflow points) concentration or salinity must be determined. Inflow points generally produce distinctive signatures in

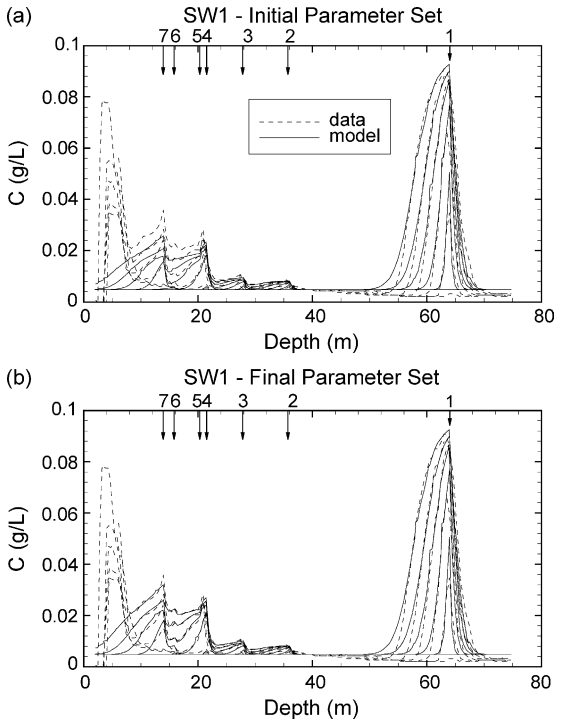

Fig. 15. Comparison of observed and simulated concentration profiles for Raymond well SW1 for (a) the initial parameter set (upper portion of Table 2), obtained by analysis of observed concentration profile signatures; and (b) the final parameter set (lower portion of Table 2), obtained by trial-and-error fitting with BORE II.

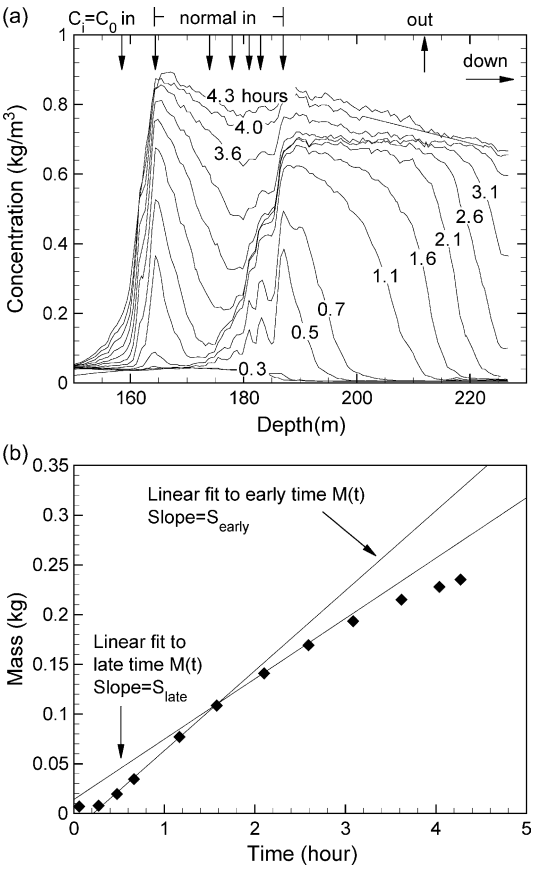

Fig. 17. Use of the mass-integral method to identify an outflow point: (a) observed $C(z)$ profiles; and (b) $M(t)$ integral along with linear fits to early and late points.

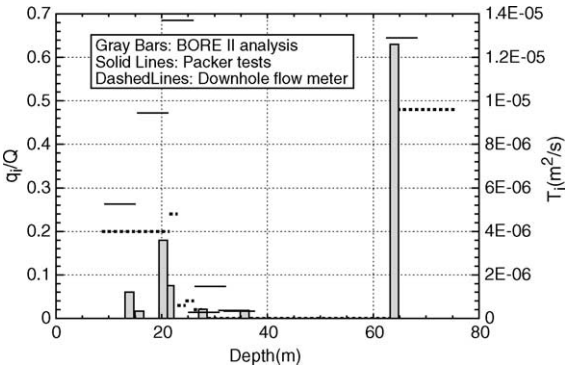

Fig. 16. Comparison of feed point flow rates q_i obtained with the flowing FEC logging method using BORE II and measurements from packer tests and a downhole flow meter (Cohen, 1995), for Raymond well SW1. The q_i values are normalized by $Q=\Sigma q_i$.

the concentration profiles $C(z)$ obtained directly from the FEC logs for the range of conditions discussed in this paper. These are summarized in Fig. 18. Both early- and late-time $C(z)$ profiles provide information on inflow points, and special conditions such as time-varying flow rate or concentration can be identified. In contrast, outflow points often do not manifest themselves clearly in $C(z)$ profiles, requiring the mass-integral analysis method described in this paper. In this method, $C(z)$ profiles are integrated over the entire borehole length to produce the ion mass in place, or mass integral, at a given time, $M(t)$. $M(t)$ is then plotted as a function of time, and the breaks in slope of $M(t)$ are used to identify outflow points. This procedure is also illustrated in Fig. 18.

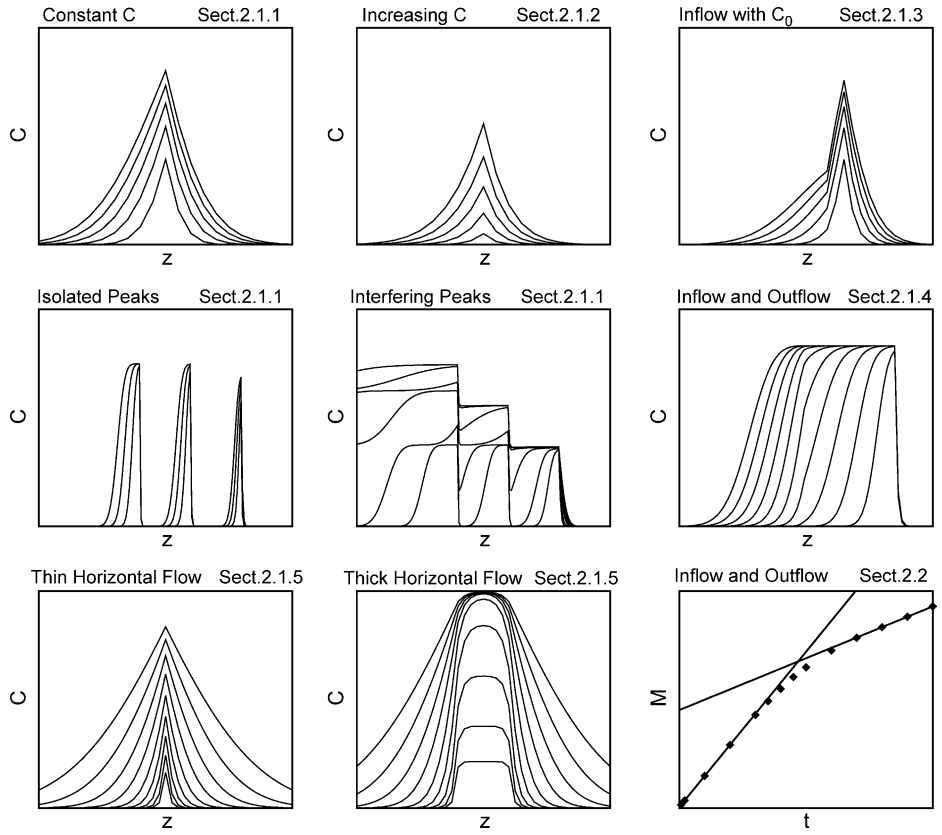

Fig. 18. Overview of the $C(z)$ and $M(t)$ signatures discussed in this paper, along with the section number where each is presented.

An understanding of the signatures produced by various flow conditions leads to the following recommendations concerning the operation and analysis of flowing FEC logging:

1. Start logging as soon as possible after de-ionized water is emplaced so that the first flow logs show individual peaks that do not interfere with one another, thus enabling peak locations and the area under individual peaks to be unambiguously determined.
2. If possible, continue logging long enough for steady-state conditions to develop. Concentration plateaus for isolated peaks ($C_{\mathrm{mid}i}$) and interfering peaks ($C_{\mathrm{max}i}$) may be used with mixing rules to determine individual feed-point flow rates and concentrations.
3. Repeat logging several times with one or two other pumping rates (e.g. half and double the original pumping rate). The manner in which FEC peaks change with Q provides information not only on the flow rate of the feed points, but on the hydraulic transmissivity and far-field pressure head conditions of the fractures or permeable layers.
4. Packing off the bottom of the wellbore interval being studied (i.e. eliminating the possibility of upflow from below) is recommended if it is a practical field operation. Knowing upflow is zero reduces uncertainty for most analyses (Fig. 3d illustrates one exception). In particular, if upflow is large compared to q_i, translation of peaks is dominated by upflow and it becomes difficult to individually determine the q_i and C_i for a given $q_i(C_i - C_0)$ product.
5. For the analysis of horizontal flow, the initial series of logging runs should be done with as low a pumping rate as possible (or zero rate), to enable visual identification of the non-skewed peaks

indicating horizontal flow Q_0. Subsequent logging with a relatively large pumping rate (at least $2Q_0$) encourages a C_{max} plateau to develop, which in turn enables an improved estimate of Q_0 to be made. Comparison to the Drost et al. (1968) analytical solution (for thick layers) or BORE II results (for thin layers or individual fractures) can further constrain Q_0.

6. In order to create a successful automated inverse method for systems including both inflow and outflow feed points, it should be beneficial to minimize not only the misfit between modeled and observed FEC logs (or equivalently, $C(z)$ profiles) but also the misfit between the modeled and observed mass integral $M(t)$ curves.

The recommended procedure for the analysis of flowing FEC logs involves first studying inflow points with $C(z)$, using the area under individual peaks and plateau concentrations. Next, outflow points are investigated by calculating $M(t)$ over the entire profile and examining the breaks in slope. Then, logs with different pumping rates can be used to infer more about feed-point properties. All of these steps are carried out in conjunction with numerical simulations using BORE II, which is also used to optimize or refine the feed-point flow rates and salinities. For convenience in field applications, the above procedure has also been formulated in flow chart form, providing step-by-step guidelines for the analysis of flowing FEC logs (Doughty and Tsang, 2002).

Finally, properties inferred from flowing FEC logging should be evaluated in the context of other geological, hydrological, geophysical, and geochemical analyses available for the site. Such systematic studies of flowing FEC logs not only yield parameter values for hydraulic properties of fractures or permeable layers, but also provide insight into flow and transport processes occurring at the site.

Acknowledgements

Discussions with Stratis Vomvoris of NAGRA, Switzerland, at the initial stage of this work were appreciated. We thank him and Kenzi Karasaki and Rob Trautz of Lawrence Berkeley National Laboratory (LBNL) for carefully reviewing this paper. Additionally, anonymous reviewers provided comments that greatly improved the paper. We are also grateful to K. Karasaki of LBNL and G. Bauer of Colog, Inc., for making their sample data sets available to us. This work was jointly supported by the Underground Injection Control Program, Office of Ground Water and Drinking Water, US. Environmental Protection Agency and by the Japan Nuclear Cycle Research Institute (JNC) under a binational agreement between JNC and US, Department of Energy (DOE), Office of Environmental Management, Office of Science and Technology, under DOE contract DE-AC03-76SF00098.

Appendix A. Governing equations

The principal equation governing wellbore FEC variation during flowing FEC logging is the one-dimensional advection-dispersion equation for the transport of mass (or ion concentration) in the wellbore. However, additional consideration must be given to the determination of FEC as a function of ion concentration and the temperature dependence of FEC.

A.1. FEC as a function of concentration

The relationship between ion concentration and FEC is reviewed, for example, by Shedlovsky and Shedlovsky (1971), who give graphs and tables relating these two quantities. Hale and Tsang (1988) made a sample fit for the case of NaCl solution at low concentrations and obtained

$$\mathrm{FEC} = 1,870\,C - 40\,C^2, \tag{A1}$$

where C is ion concentration in kg/m^3 ($\approx$g/L) and FEC is in μS/cm at 20 °C. The expression is accurate for a range of C up to $\sim$6 kg/m^3 and FEC up to 11,000 μS/cm. The quadratic term can be dropped for values of C up to $\sim$4 kg/m^3 and FEC up to 7,000 μS/cm, in which case the error will be less than 10%.

Fracture fluids typically contain a variety of ions, the most common being Na^+, Ca^{2+}, Mg^{2+}, Cl^-, SO_4^{2-}, and HCO_3^-. If a hydrochemical analysis has been completed, various methods are available for

computing an equivalent NaCl concentration for other ions. Schlumberger (1984) presents charts of multiplicative factors that convert various solutes to equivalent NaCl concentrations with respect to their effect on FEC.

A.2. Temperature dependence of FEC

In the present work, calculations are made assuming a uniform temperature of 20 °C throughout the wellbore. Actual wellbore temperatures generally vary with depth, so temperature corrections must be applied to field FEC data to obtain values at a constant temperature for comparison with model output.

The effect of temperature T on FEC can be accounted for using the following equation (Schlumberger, 1984), which provides the equivalent FEC values at 20 °C:

$$\mathrm{FEC}(20\,^{\circ}\mathrm{C}) = \frac{\mathrm{FEC}(T)}{1 + S(T - 20\,^{\circ}\mathrm{C})}, \tag{A2}$$

where $S = 0.024\,^{\circ}\mathrm{C}^{-1}$. Typical FEC logging tools measure T and FEC at each depth, making application of Eq. (A2) straightforward.

A.3. Advection–dispersion equation

The advection–dispersion equation describes the evolution of ion concentration as a function of space and time in a wellbore containing multiple feed points, given the pumping rate of the well, the inflow or outflow rate of each feed point, its location, and, for inflow points, its ion concentration. Fluid flow is assumed to be steady, with transport occurring by longitudinal advection and dispersion along the wellbore and instantaneous mixing of feed-point fluid in the plane of the wellbore cross section. These assumptions allow use of a one-dimensional model; the differential equation for mass or solute transport in a wellbore is:

$$\frac{\partial}{\partial z}\left(D_o \frac{\partial C}{\partial z}\right) - \frac{\partial}{\partial z}(Cv) + S = \frac{\partial C}{\partial t}, \tag{A3}$$

where z is depth, t is time, and C is ion concentration. The first term is the dispersion term, with D_0 the dispersion coefficient in m^2/s, the second term is the advective term, with v the fluid velocity in m/s, and S is the source term in $\mathrm{kg/m}^3\,\mathrm{s}$. The coefficient D_0 includes contributions from molecular diffusion and dispersive mixing of wellbore fluid. The movement of the electric conductivity logging tool up and down the wellbore greatly enhances the longitudinal dispersion coefficient D_0 over the value for still water. This one-dimensional partial differential equation is solved numerically using the finite-difference method, with upstream weighting applied in the advective term. The following initial and boundary conditions are specified:

$$\begin{aligned} &C(z,0) = C_0(z), \\ &C(z_{\min},t) = C_0(z_{\min}) \text{ for flow into the wellbore from above,} \\ &C(z_{\max},t) = C_0(z_{\max}) \text{ for flow into the wellbore from below,} \\ &D_0 = 0 \text{ for } z < z_{\min} \text{ and } z > z_{\max}, \end{aligned} \tag{A4}$$

where $z_{\min}$ and $z_{\max}$ are the upper and lower limits of the wellbore interval being studied. The first condition allows for the specification of initial ion concentrations in the wellbore. In this paper, we consider C_0 a constant independent of Z. The second and third conditions allow for advective flow of ions into the wellbore interval from above and below. The final condition ensures that diffusion and dispersion do not take place across the boundaries of the wellbore interval. In general, advection will be the dominant process at the boundaries. If diffusion or dispersion is dominant for a particular problem, the boundaries should be extended to prevent improper trapping of electrolyte.

References

Aquilina, L., Eberschweiler, C., Perrin, J., 1996. Comparison of hydrogeochemical logging of drilling fluid during coring with the results from geophysical logging and hydraulic testing: Example of the Morte–Mérie scientific borehole, Ardèche-France, Deep Geology of France Programme. J. Hydrol. 185, 1–21.

Bauer, G.D., LoCoco, J.J., 1996. Hydrogeophysics determines aquifer characteristics. Int. Ground Water Technol. August/-September, 12–16.

Cohen, A.J.B., 1993. Hydrogeologic characterization of a fractured granitic rock aquifer, Raymond, California, MSc Thesis, University of California, Berkeley, 97 pp.

Cohen, A.J.B., 1995. Hydrogeologic characterization of fractured rock formations: A guide for groundwater remediators, Rep.

LBL-38142, Lawrence Berkeley National Laboratory, Berkeley, CA (available on-line at http://www-library.lbl/docs/LBL/381/42/PDF/LBL-38142.pdf).

Doughty, C., Tsang, C.-F. 2000. BORE II—A code to compute dynamic wellbore electrical conductivity logs with multiple inflow/outflow points including the effects of horizontal flow across the well, Rep. LBNL-46833, Lawrence Berkeley National Laboratory, Berkeley, CA (available on-line at http://www-library.lbl/docs/LBNL/468/33/PDF/LBNL-46833.pdf).

Doughty, C., Tsang, C.-F. 2002. Inflow and outflow signatures in flowing wellbore electrical-conductivity logs, Rep. LBNL-51468. Berkeley, CA: Lawrence Berkeley National Laboratory (available on-line at http://www-library.lbl.gov/docs/LBNL/514/68/PDF/LBNL-51468.pdf).

Drost, W., Klotz, D., Koch, A., Moser, H., Neumaier, F., Rauert, W., 1968. Point dilution methods of investigating ground water flow by means of radioisotopes. Water Resour. Res. 4 (1), 125–146.

Evans, D.G., 1995. Inverting fluid conductivity logs for fracture inflow parameters. Water Resour. Res. 31 (12), 2905–2915.

Evans, D.G., Anderson, W.P., Jr., Tsang, C.-F., 1992. Borehole fluid experiments near salt contamination sites in Maine, in proceedings of the NGWA Conference on Eastern Regional Ground Water Issues, Boston. pp. 797–807.

Guyonnet, D., Rivera, A., Löw, S., Correa, N., 1993. Analysis and synthesis of fluid logging data from Wellenberg boreholes SB1, SB3, SB4 and SB6, Nagra Tech. Rep. NTB 92-01, pp. 153, Nagra, Wettington, Switzerland.

Hale, F.V., Tsang, C.-F., 1988. A code to compute borehole conductivity profiles from multiple feed points, Rep. LBL-24928, Lawrence Berkeley Laboratory, Berkeley, CA.

Karasaki, K., Freifeld, B., Cohen, A., Grossenbacher, K., Cook, P., Vasco, D., 2000. A multidisciplinary fractured rock characterization study at Raymond field site, Raymond, CA. J. Hydrol. 236, 17–34.

Kelley, V.A., Lavanchy, J.M., Löw, S., 1991. Transmissivities and heads derived from detailed analysis of Siblingen 1989 fluid logging data, Nagra Tech. Rep. NTB 90-09, pp. 184, Nagra, Wettington, Switzerland.

Keys, W.S., 1989. Borehole geophysics applied to groundwater investigations. National Water Well Association, Dublin, Ohio.

Löw, S., Tsang, C.-F., Hale, F.V., Hufschmied, P. 1990. The application of moment methods to the analysis of fluid electrical conductivity logs in boreholes, Rep. LBL-28809, Lawrence Berkeley Laboratory, Berkeley, CA.

Löw, S., Kelley, V., Vomvoris, S., 1994. Hydraulic borehole characterization through the application of moment methods to fluid conductivity logs. J. Appl. Geophys. 31 (1-4), 117–131.

Marschall, P., Vomvoris, S., 1995. (editors), Grimsel Test Site: Developments in hydrotesting, fluid logging and combined salt/heat tracer experiments in the BK Site (Phase III), Nagra Tech. Rep. 93–47, Nagra, Wettingen, Switzerland.

National Research Council Committee on Fracture Characterization and Fluid Flow, 1996. Rock fractures and fluid flow: contemporary understanding and applications, National Academy Press, Washington, DC.

Paillet, F.L., Pedler, W.H., 1996. Integrated borehole logging methods for wellhead protection applications. Eng. Geol. 42 (2-3), 155–165.

Pedler, W.H., Head, C.L., Williams, L.L. 1992. Hydrophysical logging: A new wellbore technology for hydrogeologic and contaminant characterization of aquifers, National Outdoor Action Conference, National Ground Water Association, Las Vegas, Nevada.

Schlumberger, Ltd, 1984. Log interpretation charts, New York.

Shedlovsky, T., Shedlovsky, L., 1971. Conductometry, in Physical Methods of Chemistry, Part IIA: Electrochemical Methods, in: Weissberger, A., Rossiter, B.W. (Eds.),. Wiley, New York, pp. 164–171.

Tsang, C.-F., Doughty, C., 2003. Multi-rate flowing fluid electric conductivity logging method. Water Resour. Res. 39 (12), 1354. 10.1029/2003WR002308.

Tsang, C.-F., Hale, F.V., 1989. A direct integral method for the analysis of borehole fluid conductivity logs to determine fracture inflow parameters. Proceedings of the National Water Well Conference on New Field Techniques for Quantifying the Physical and Chemical Properties of Heterogeneous Aquifers, Dallas, Texas, March 20-23, Rep. LBL-27930, Lawrence Berkeley Laboratory, Berkeley, CA.

Tsang, C.-F., Hufschmeid, P., Hale, F.V., 1990. Determination of fracture inflow parameters with a borehole fluid conductivity logging method. Water Resour. Res. 26 (4), 561–578.

Ward, R.S., Williams, A.T., Barker, J.A., Brewerton, L.J., Gale, I.N. 1998. Groundwater tracer tests: a review and guidelines for their use in British aquifers, R & D Technical Report W160, Environment Agency, UK.